

Experimental investigation of Lévy flights for step-length distributions with a length-dependent local power exponent.

Isaac C. Nunes ^{1,2} Jesús P. López ¹ and Thierry Passerat de Silans ^{1,*}

¹*Departamento de Física, CCEN, Universidade Federal da Paraíba,
Caixa Postal 5008, 58051-900 João Pessoa, Paraíba, Brazil*

²*Departamento de Física, Universidade Federal de Pernambuco, 50670-901 Recife, Pernambuco, Brazil*
(Dated: March 10, 2026)

We experimentally investigate the transmission of light by dense atomic vapor. The light propagating in dense atomic vapor can be modeled as a Lévy flight random walk. For such system, the step-length distribution can be modeled as $P(\ell) \sim \ell^{-1-\alpha(\ell)}$, with the Lévy index $\alpha(\ell)$ varying smoothly with the step length. Moreover, the walkers alternate between two distinct distributions depending on the occurrence of collisions between atoms in the light scattering. We obtain the Lévy index from transmission measurements for different system sizes and atomic densities. The measured Lévy index is determined by the system size $\alpha = \alpha(\ell = L)$. Simulations are made for walkers alternating between two Lévy like step-length distributions.

I. INTRODUCTION

Lévy flight is a kind of random walk with a step-length distribution with divergent variance. Lévy flight are often modeled by a step-length distribution that decays asymptotically as a power law $P(\ell) \sim \ell^{-1-\alpha}$, with the Lévy index $\alpha \leq 2$. The main feature of Lévy flight is the occurrence of large steps that, although rare, dominate the dynamics of the random walk. For example, the large steps lead the transmission by a sample of thickness L to decay as $L^{-\alpha/2}$, slower than that for normal diffusion [1–4]. Lévy flights are present in a variety of systems, just to name a few: animal foraging [5], phonons transport in nanowires [6] and spread of genes lineage [7].

Multiple scattering of light by atomic resonant vapor can be described as a Lévy flight random walk [8, 9], the step length being the distance traveled by a photon between successive scatterings. In the scattering process, the light's frequency is redistributed, leading to the Lévy flight's typical large step performed by light scattered off-resonance. Experimental investigations of Lévy flight of light in atomic vapor have been concentrated on determining the Lévy index α from transmission measurements [2, 10–14]. The step-length distribution for light in atomic vapor is not a power law [14–17] but could be modeled as:

$$P(\ell) \sim \ell^{-1-\alpha(\ell)}, \quad (1)$$

with the Lévy index $\alpha(\ell)$ slowly varying with the step length. The smooth variation of $\alpha(\ell)$ with ℓ allows us to describe the step-length distribution locally as a power law with local exponent $\alpha(\ell)$. Measurements of α from transmission have evidenced a dependence of α on the size of the system [13, 14]. Moreover, the steps alternate between two different step-length

distributions, related to two different cases of frequency redistribution [15, 18, 19], depending on whether or not a collision between atoms has occurred during the photon scattering process.

In the present article, we investigate experimentally the transmittance of light by a resonant atomic cesium vapor. Our aim is twofold: i) to determine if the local exponent of the step-length distribution is retrieved from transmission measurements and ii) to obtain information of how the alternation between two distinct step-length distributions influences the transmission through a sample. Simulations are made to confirm the experimental results.

The article is organized as follows: in section II we discuss the frequency redistribution, giving emphasis to the existence of two distinct cases, whether there are or not collisions between atoms during the scattering event. Furthermore, we describe how the frequency redistribution influences the step-length distribution of the random walk. In section III we describe the experiment and discuss the experimental results. In section IV, we describe simulations of Lévy flight random walk with length dependent power law exponent and two distinct distributions. In section V, we compare and discuss the results of experiment and simulations and, finally, conclude in section VI.

II. FREQUENCY REDISTRIBUTION FOR LIGHT SCATTERED BY AN ATOMIC VAPOR

The light scattered by resonant alkali atomic vapor has its frequency redistributed by two main mechanisms: (i) Doppler shifts and (ii) atomic elastic collisions that randomize the atomic dipole phase [15, 20, 21]. This frequency redistribution results in a broadened scattered spectrum with each frequency interacting with the vapor with a different cross-section. The larger the detuning to atomic resonance, the lower is the cross-section, and the

* thierry@otica.ufpb.br

higher is the probability of large distance traveled before a new scattering event. The step-length distribution is related to the interaction cross-section $\sigma(x')$ and to the scattered spectral profile $\Theta(x')$ by:

$$P_n(\ell) = \int dx' \Theta_n(x') \beta(x') e^{-N\sigma(x')\ell}, \quad (2)$$

where x' denote the scattered detuning normalized by Doppler width, N is the atomic density and $\beta(x) = N\sigma(x)$ is the absorption coefficient. The scattered spectral profile depends on the scattering event number, n , and on the incident detuning x and can be calculated using a recurrence rule [11, 17]:

$$\Theta_n(x') = \int dx C(x) \Theta_{n-1}(x) \frac{R(x', x)}{\phi(x)}, \quad (3)$$

with $\Theta_{n-1}(x)$ the scattered profile at step $n-1$, $C(x)$ a system size dependent extinction factor that computes the probability of the photon with detuning x to be scattered by the vapor. $\phi(x)$ is a normalized absorption profile ($\int dx \phi(x) = 1$) and $R(x, x')$ is a joint frequency redistribution function [18]. Hummer [18], has calculated the joint redistribution function for four cases, two of which will be considered here for scattering by alkali vapor: (i) case II, for pure natural broadening (no collisions), and (ii) case III, for combined natural and collisional broadening. Both cases II and III are also Doppler broadened in the laboratory rest frame.

For finite vapor system, $\Theta_n(x')$ stabilizes after some scattering events [17] with the scattering profile for case II converging to a Doppler profile and case III converging to a Voigt profile with heavy tailed Lorentzian wings, that favors the occurrence of large steps [22]. The frequency redistribution function can be written as a weighted average [19, 23–25]:

$$R(x, x') = (1 - P_C) R_{II}(x, x') + P_C R_{III}(x, x'), \quad (4)$$

with $P_C = \frac{\Gamma_C}{\Gamma_C + \Gamma_n}$ being the probability that a collision between atoms occurs during a scattering event [24, 25]. Γ_C and Γ_n denote collisional and natural widths, respectively.

The photons can undergo some scattering events before a collision between the atoms occurs. During its random walk, the photons intercalate between the two distinct step-length distributions corresponding to $P_{II}(\ell)$ for scattering with no collision between atoms (case II) and $P_{III}(\ell)$ if a collision occurs during the scattering (case III).

$$P(\ell) = \begin{cases} P_{II}(\ell), & \text{if no collisions occurs during scattering} \\ P_{III}(\ell), & \text{if collision occurs during scattering.} \end{cases} \quad (5)$$

From the calculated step-length distributions and from Eq. 1, we can extract the local power law exponent

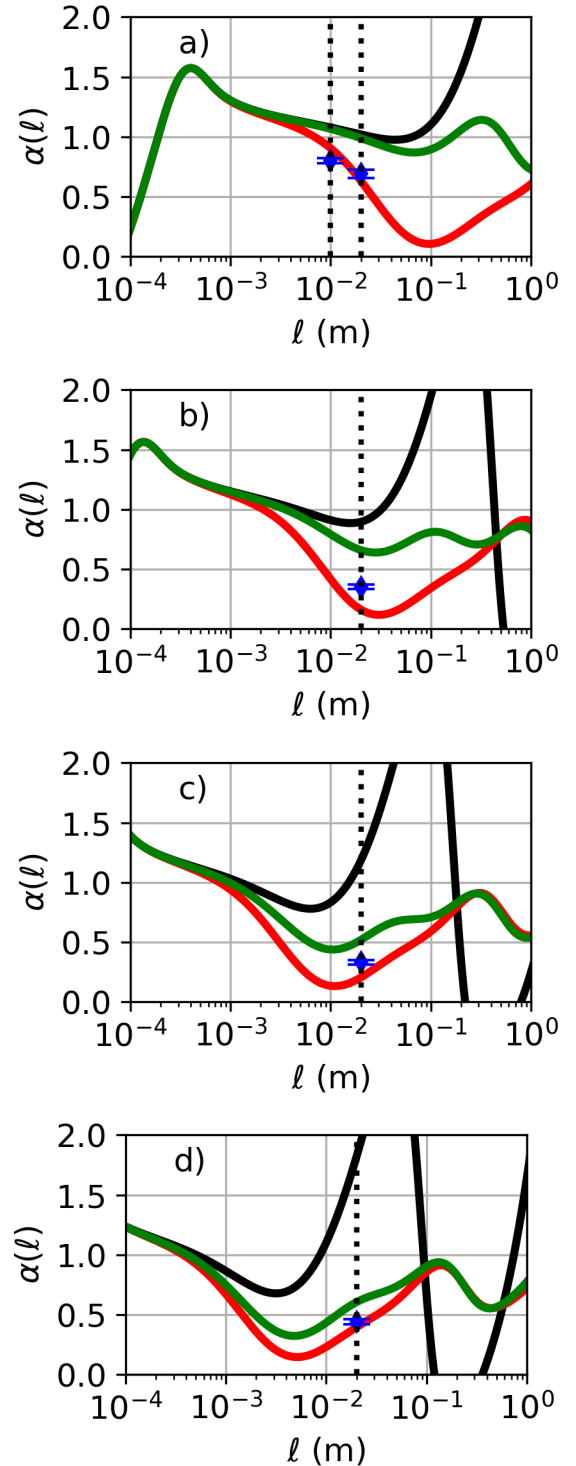


FIG. 1. Measured Lévy index for different atomic densities (diamonds). Lines are step-length-dependent Lévy index $\alpha(\ell)$ calculated from $P_{II}(\ell)$ (black lines), $P_{III}(\ell)$ (red lines) and $P(\ell)$ (green lines). (a) For density $N = 3.5 \times 10^{12}$ atoms/cm³ corresponding to $P_C = 6\%$; (b) for $N = 10 \times 10^{12}$ atoms/cm³ and $P_C = 15\%$; (c) for $N = 25 \times 10^{12}$ atoms/cm³ and $P_C = 30\%$; (d) for $N = 44 \times 10^{12}$ atoms/cm³ and $P_C = 43\%$. For density (a) measurement were made for two different cells of thickness $L = 1$ cm and $L = 2$ cm. For densities (b-d) only the cell of thickness $L = 2$ cm were used.

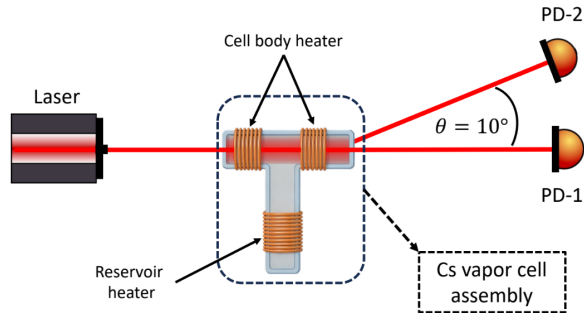


FIG. 2. Scheme of the experimental set-up. A low power laser beam is incident on the atomic vapor and diffuse transmission is collected by photodetector PD2 at 10° relative to laser beam.

$1 + \alpha(\ell) = -\frac{d\log_{10}(P(\ell))}{d\log_{10}(\ell)}$. In Fig. 1 we show $\alpha(\ell)$ calculated from $P_{II}(\ell)$, $P_{III}(\ell)$ and $P(\ell)$ for different atomic densities. Looking, for instance, at Fig. 1(a) we see that $\alpha(\ell)$ for case II varies smoothly with ℓ keeping in a range $1.2 \leq \alpha \leq 1.0$ for a wide range of step lengths (from 2 mm to 3 cm). For case III, α decreases to values as low as $\alpha \sim 0.1$ related to the transition from the Doppler core of the scattering profile to the Lorentzian wings and increases to $\alpha \sim 0.5$ for larger steps related to the Lorentzian wings of the scattering profile [8, 14, 16, 17]. The $\alpha(\ell)$ calculated from the total step-length distribution $P(\ell)$ in Fig. 1(a) ($P_C \sim 6\%$) approaches the case II for steps with $\ell < 10^{-1}$ m, as collisions between atoms are rare. However, for large steps, the $P(\ell)$ distribution approaches the $P_{III}(\ell)$ distribution, since there is a cut-off in the $P_{II}(\ell)$ distribution [15, 17] consequence of the scattering coherence in the atomic rest frame.

III. EXPERIMENT

The experimental set-up is shown in Fig 2. A laser beam with wavelength of 852 nm is incident on a cesium vapor contained in a sealed cell and scanned around the D_2 line. Two independent ovens heat the cell's probed volume and the liquid cesium reservoir. The density of the vapor is increased by heating the reservoir such that the optical density at the line center is a minimum of 60; that is, there is no ballistic transmission around the line center. The light might undergo multiple scattering events before escaping the vapor and is collected as a diffuse transmission by detector PD2. Detector PD2 is at an angle of 10° related to the laser beam axis and is placed past a lens to collect diffuse light. More details of the experimental parameters are given in the appendix.

Our experimental aim is to measure the diffuse transmission for fixed atomic density N and cell thickness L as a function of the starting point of the random walk z_0 .

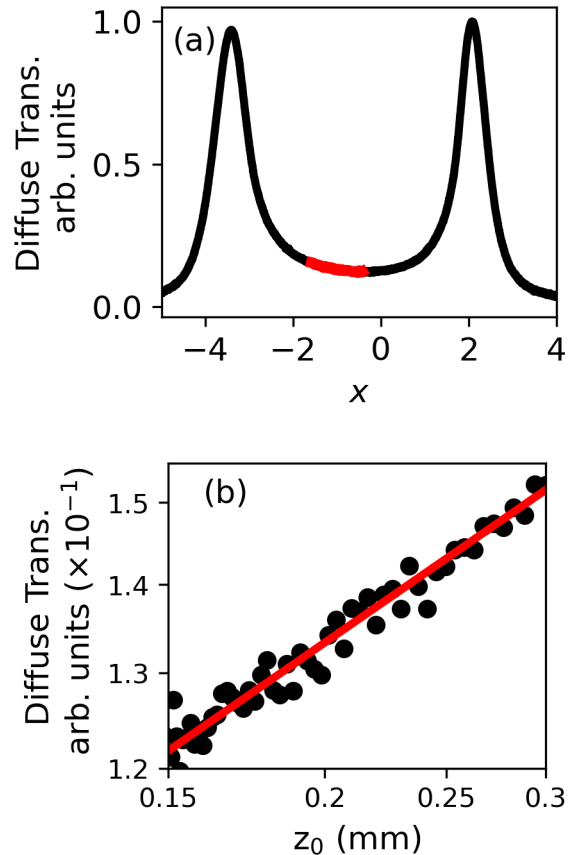


FIG. 3. (a) Diffuse transmission spectrum for a cell of thickness $L = 2$ cm and atomic density of $N = 3.5 \times 10^{12}$ atoms/cm³. The zero detuning corresponds to the $6S_{1/2}(F = 4) \rightarrow 6P_{3/2}(F' = 5)$ transition. (b) Power law dependence of diffuse transmission as a function of laser penetration depth z_0 . The range of frequencies analysed in (b) corresponds to red-solid line in (a).

Diffuse transmission is expected to scale as [3, 4]:

$$T_D \propto \left(\frac{z_0}{L}\right)^{\alpha/2}. \quad (6)$$

In our experiment, the laser frequency is scanned around the $6S_{1/2}(F = 4) \rightarrow 6P_{3/2}(F' = 3, 4, 5)$ cesium transitions with the starting point of the random walk defined as the penetration depth of the laser beam given by $z_0 = (N\sigma(x))^{-1}$ [14]. An example of diffuse transmission spectrum is shown in Fig. 3. The frequency axis of the spectrum in Fig 3(a) can be transformed into the penetration depth axis to build Fig. 3(b), which shows a power law dependence of diffuse transmission as a function of the starting point of the random walk as predicted in Eq. 6. Diffuse transmission is fitted by a power law to obtain the Lévy index α . The results of measured α for two different cells of thickness $L = 1$ cm and $L = 2$ cm for the same atomic density of $N = 3.5 \times 10^{12}$ atoms/cm³ are

shown as diamonds in Fig. 1(a). The Results for three other densities for $L = 2$ cm are shown in Figs. 1(b-d)[26]

Two main results are evidenced in Fig. 1: i) The measured values α depend on the system size and follow the curve $\alpha(\ell)$; ii) the measured α follow the expected curve $\alpha(\ell)$ for the case *III*, that is, for scattering with collisions between atoms even if the collisional width is small relative to the natural width ($\Gamma_C \sim 0.1\Gamma_n$ for Fig. 1(a)).

IV. SIMULATIONS

A. Double Pareto distribution

As a tentative way to understand both the influence of a step-length distribution with varying local power exponent and the alternation between two step-length distributions, we simulate a random walk in one dimension following the distributions $P^{DP}(\ell)$:

$$P^{(DP)}(\ell) = \begin{cases} P_{II}^{(P)}(\ell), & \text{with probability } 1 - P_C \\ P_{III}^{(P)}(\ell), & \text{with probability } P_C \end{cases}, \quad (7)$$

with $P_{(II,III)}^{(P)}(\ell)$ being normalized Pareto distributions:

$$P_{(II,III)}^{(P)}(\ell) = \frac{\alpha_{(II,III)}}{\ell_0} \left(\frac{\ell_0}{\ell} \right)^{1+\alpha_{(II,III)}} \Theta(\ell - \ell_0), \quad (8)$$

with Θ the Heaviside function and ℓ_0 the minimum step length. The Lévy indexes of the distributions are chosen such that $1 < \alpha_{II} < 2$ and $0 < \alpha_{III} < 1$ to mimic the two step-length distribution for light diffusing in atomic vapor corresponding to Doppler and Voigt scattering profiles (cases II and III), respectively.

1. Transmission as a function of starting point

The walker evolves in a 1D space $0 < z < L$ with starting point of the random walk z_0 obeying $\ell_0 \ll z_0 \ll L$, the so-called *continuous limit* [4]. We run the simulation for fixed ℓ_0 and L for various starting points z_0 . We collect the transmission, T , through the absorbing wall at $z = L$ as a function of z_0 , see Fig. 4(a). Then, using Eq. 6, we determine the local slope of $\log_{10}(T)$ as a function of $\log_{10}(z_0)$ to obtain $\alpha/2$. The obtained values of α using this procedure for two different system sizes are shown in Fig. 4(b). We have run the simulation with $\ell_0 = 1$, $L = 10^3$ and $L = 10^5$ and z_0 ranging from 10 to $L/10$.

The obtained values of α depend on the starting point z_0 and do not depend on the size of the system L . As the distance from the starting point to the absorbing wall at $z = 0$ is much less than the distance to $z = L$ the

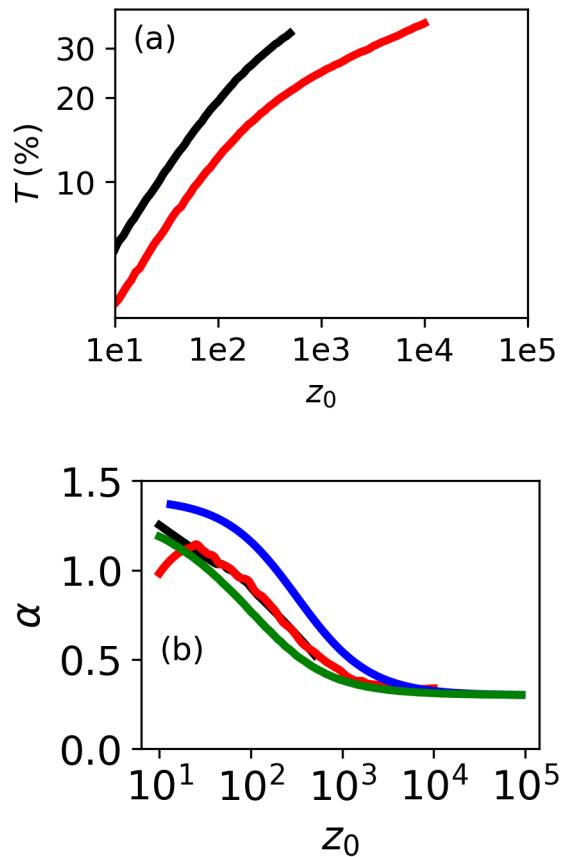


FIG. 4. (a) Transmission as a function of starting point z_0 for two different sizes of system: $L = 5 \times 10^3$ (black-solid line) and $L = 10^5$ (red-solid line). (b) Local Lévy exponent α obtained by fitting locally Eq. 6 for $L = 5 \times 10^3$ (black-solid line) and $L = 10^5$ (red-solid line). In blue-solid line we plot expected α value calculated from the step-length distribution: $1 + \alpha = -\frac{d \log(P^{(DP)})}{d \log(z_0)}$. In green-solid line we plot expected $\alpha^{(w)}$ obtained from Eq. 9

majority of the walkers escape the system on the left side. As $T + T^{(left)} = 1$ the transmission by $z = L$ is strongly influenced by the number of particles that escape by $z = 0$ (denoted by $T^{(left)}$), which should depend on z_0 and very little on the large system size L . We conclude that T is governed by $T^{(left)}$, which depends on the starting point z_0 and not on the size of the system L . Hence, the obtained values of α from the simulations should be related to the local slope of $P^{(DP)}$ around z_0 , calculated from $1 + \alpha = -\frac{d \log(P^{(DP)})}{d \log(z_0)}$, which we plot as a blue line in Fig. 4. The local slope follows quite well the dependence of α obtained from the simulations, which reaffirms the argument that $T^{(left)}$ rules the dynamics.

From the simulations, we can compute the number of walkers that have escaped by $z = 0$ after a step corresponding to $P_{II}^{(P)}$ or $P_{III}^{(P)}$. We denote those numbers by N_{II} and N_{III} , respectively. We have estimated a

weighted $\alpha^{(w)}$ value by:

$$\alpha^{(w)}(z_0) = \frac{N_{II}(z_0)}{N_{II}(z_0) + N_{III}(z_0)} \alpha_{II} + \frac{N_{III}(z_0)}{N_{II}(z_0) + N_{III}(z_0)} \alpha_{III}. \quad (9)$$

$\alpha^{(w)}$ is plotted as a green-solid line in Fig. 4. It follows quite well the obtained α values.

2. Transmission as a function of minimum step length

We have also tested in the simulations the regime for which $z_0 \ll \ell_0 \ll L$ [4] by fixing z_0 to 10^{-3} and running simulations for ℓ_0 ranging from 1 to 5 [27]. The simulated diffuse transmission T as a function of ℓ_0 is shown in Fig. 5(a) for different system sizes. It is clear that the diffuse transmission follows the power law given by [4]:

$$T \propto \left(\frac{\ell_0}{L}\right)^{\alpha/2}. \quad (10)$$

From Eq. 10 we can extract α from the simulated T . The α values clearly depend on the size of the system, and we plot the α values obtained from simulations in Fig. 5(b) together with the local exponent of the step-length distribution for step of size $\ell = L$, calculated from $1 + \alpha(L) = -\frac{d \log_{10}(P(L))}{d \log_{10}(L)}$. The obtained α from the simulations closely follow the local exponent of the step-length distribution for $\ell = L$. Also plotted in Fig. 5(b) is a weighted α value taken as:

$$\alpha^{(w)} = \frac{N_{II}}{N_{II} + N_{III}} \alpha_{II} + \frac{N_{III}}{N_{II} + N_{III}} \alpha_{III}, \quad (11)$$

with N_{II} and N_{III} the number of walkers transmitted by $z = L$ after performing a step corresponding to $P_{II}^{(P)}$ and $P_{III}^{(P)}$ distributions, respectively.

B. Photon diffusion in atomic vapor

1. Description of the simulation

We simulate the photon diffusion in an atomic vapor using the Monte Carlo method. The simulation follows the sequence of steps described below. We consider a slab geometry with longitudinal axis z with absorbing boundaries at $z = 0$ and $z = L$. The photon is incident along the z axis and is first scattered at position z_0 . The velocity component parallel to the incident photon direction is taken from the distribution [28, 29]:

$$P(v_{\parallel}) \propto \frac{a^2}{a^2 + (x - v_{\parallel})^2} e^{-v_{\parallel}^2}, \quad (12)$$

with v_{\parallel} given in terms of the most probable speed and a is the Voigt parameter defined as the ratio of homogeneous

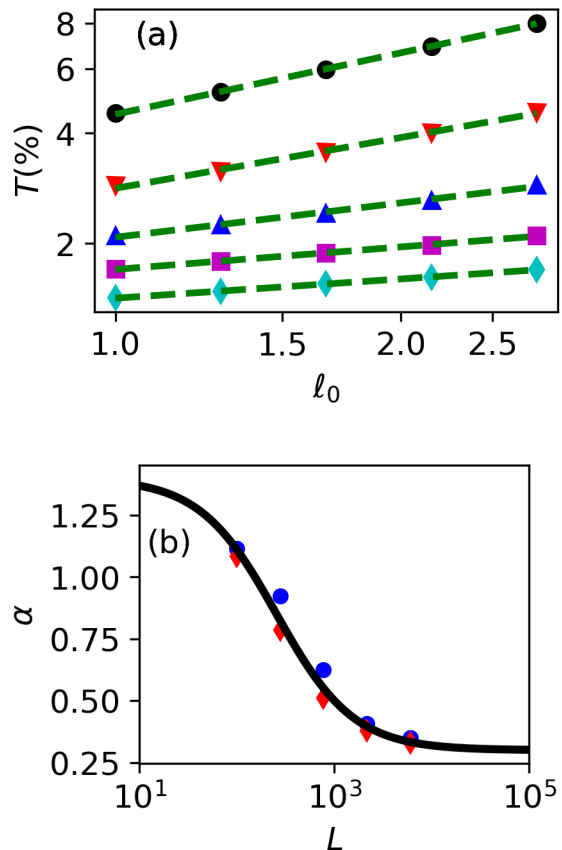


FIG. 5. Diffuse transmission as a function of ℓ_0 for different sizes of systems L : $L = 100$ (black circles), $L = 280$ (red triangle), $L = 780$ (blue triangle), $L = 2150$ (magenta squares) and $L = 6000$ (cyan diamonds). (b) Extracted Lévy index α by fitting Eq. 10 to transmission as a function of L (blue circles). Black-solid line: expected α values calculated from $1 + \alpha(L) = -\frac{d \log(P(L))}{d \log(L)}$. Red-diamonds: Expected $\alpha^{(w)}$ calculated using Eq. 11.

and Doppler width. The velocity component perpendicular to photon incident direction is taken from a two dimensional Maxwell-Boltzmann distribution. The photon detuning in the atomic rest frame, x^{at} , Doppler shifted from the laboratory frame detuning x is calculated as:

$$x^{at} = x - v_{\parallel}. \quad (13)$$

The emission in the atomic rest frame depends on the occurrence of a collision during the scattering with probability P_C . If no collision occurs, the scattered and incident detuning are the same in the atomic rest frame $x'^{at} = x^{at}$. If a collision occurs, the scattered detuning in the atomic rest frame is taken from a Lorentzian distribution [18, 19]:

$$P(x'^{at}) = \frac{a}{\pi} \frac{1}{(x'^{at})^2 + a^2}. \quad (14)$$

Then the scattered direction \vec{n}' is isotropically drawn and

the scattered detuning is Doppler shifted for the laboratory rest frame:

$$x' = x'^{at} + \vec{n} \cdot \vec{v}. \quad (15)$$

Once we have the scattered detuning we draw the distance traveled by the photon until the next scattering event following the distribution:

$$P_S(\ell) = \beta(x')e^{-\beta(x')\ell}. \quad (16)$$

The position of the photon is updated and computed as transmitted if $z > L$. If $z < 0$ the photon is lost and if $0 < z < L$ the photon is inside the vapor, and the process is restarted. For simplification of the simulation routine, we work with a two-level system and with dimensionless size. The absorption coefficient is a Voigt profile defined as [15]:

$$\beta(x) = \frac{1}{\ell_0} \frac{a}{\pi^{3/2}} \int_{-\infty}^{\infty} \frac{e^{-y^2}}{a^2 + (x - y)^2} dy. \quad (17)$$

2. Transmission as a function of starting point z_0

We simulate the photon random walk and collect diffuse transmission as a function of incident detuning, as in the experiment. The incident photon, at detuning x , penetrates the vapor a distance z_0 given by the distribution of Eq. 16. In Fig. 6 we plot diffuse transmission as a function of the mean penetration depth $\bar{z}_0 = 1/\beta(x)$ on a log-log scale. As expected, a power law behavior is obtained [4, 14, 30] (see Eq. 6) from which we extract the Lévy index α . However, the obtained values of α are in the range $0.9 < \alpha < 1.0$ and do not depend on the size of the system L even for the change of L by a factor of 10. The fact that the power dependence of T with z_0 does not depend on size of the system is similar to that found for the simulation with the Double Pareto distribution.

3. Transmission as a function of typical step-length ℓ_0

We also simulate the diffuse transmission as a function of typical step-length ℓ_0 for fixed z_0 and L . In an experiment, ℓ_0 can be changed by adjusting the atomic density, as was done in [2, 12, 13]. We perform the simulation in the limit $z_0 \ll \ell_0$, for which the diffuse transmission scales as Eq. 10. We extract the Lévy index α by fitting diffuse transmission as a power law (Eq. 10). The extracted Lévy index is then compared in Fig. 7 with theoretical predictions for α values corresponding to the local exponent of the step-length distribution (Eq. 2).

The extracted α values from the simulations follow well the theoretically predicted curves of $\alpha(\ell)$. We can clearly distinguish between the two distinct step-length distributions corresponding to coherent scattering in the atomic rest frame (case *II*) and incoherent scattering (case *III*).

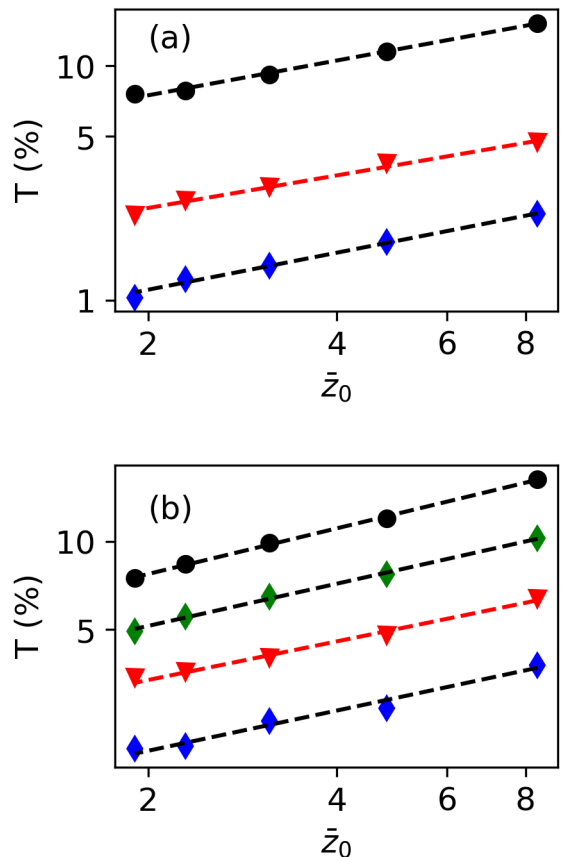


FIG. 6. Diffuse transmission as a function of mean penetration depth, \bar{z}_0 , for four different cell thicknesses: $L = 120$ (black-circles), $L = 270$ (green diamonds), $L = 540$ (red triangles) and $L = 1080$ (blue diamonds). The diffuse transmission are fitted by Eq. 6 to obtain the Lévy index α . (a) for $P_C = 0$ and (b) for $P_C = 100\%$.

Moreover, the α values depend on the system size L with the value extracted from the simulations corresponding well to $\alpha(L)$, a result similar to that obtained in the experiment.

To see the effect of different probability of collisions, we have obtained α as a function of P_C for a system of size $L = 1100$ from simulations. In Fig. 8(a) we show theoretically calculated $\alpha(\ell)$ curves for $P_C = 0, 30\%, 50\%, 70\%$ and 100% as well as the α values from simulation transmissions. The simulated values follow well the theoretical predictions. We also obtain from the simulations the percentage of photons that escape by $z = L$ after a step of case *II* (*III*), denoted as N_{II} (N_{III}), in a way similar to section IV-A, which are plotted in Fig. 8(b). The percentage of photons that escape after a step corresponding to case *III* is higher than P_C as the large steps are more common in case *III*. We estimated a weighted Lévy index as $\alpha_w = N_{II}\alpha_{II} + N_{III}\alpha_{III}$, with α_{II} (α_{III}) theoretical local exponent for case *II* (*III*) for $\ell = L$, which follows very well the extracted α from the simulations

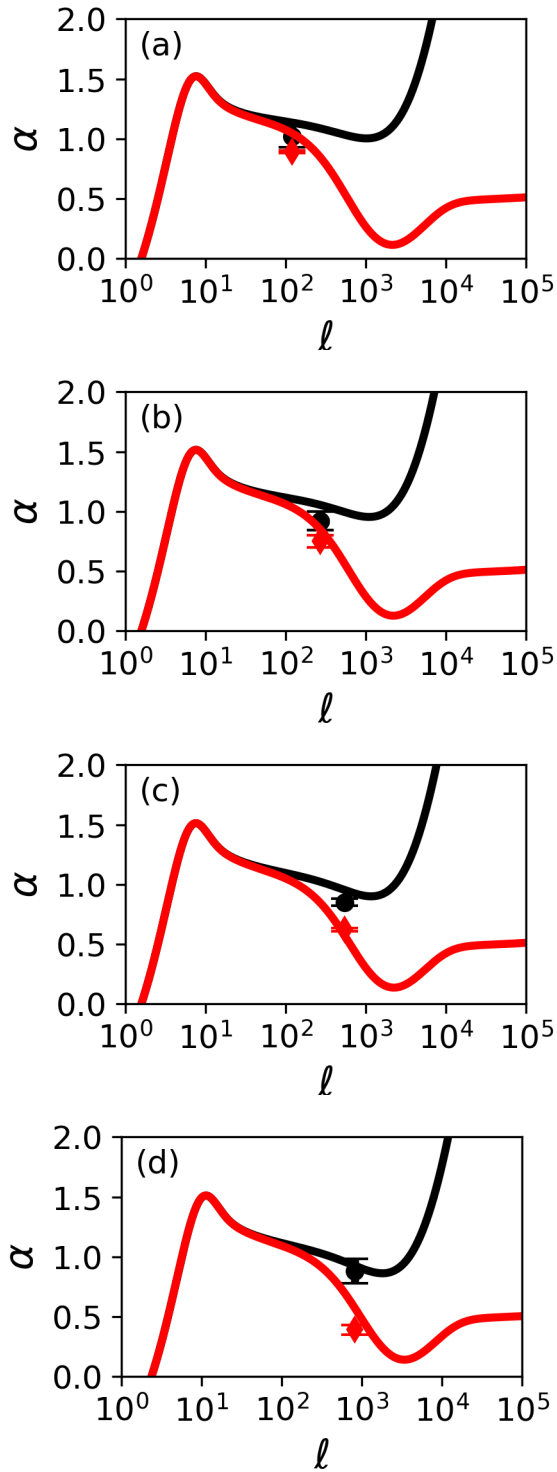


FIG. 7. Calculated local power exponent of step-length distributions for $P_C = 0$ (black-solid line) and $P_C = 100\%$ (red-solid line) for $\ell_0 = 1$ and different cell thicknesses (a) $L = 120$, (b) $L = 270$, (c) $L = 540$ and (d) $L = 810$. In each Fig., symbols are α values extracted from fitting Eq. 10 to simulated diffuse transmission.

(see Fig. 8(c)).

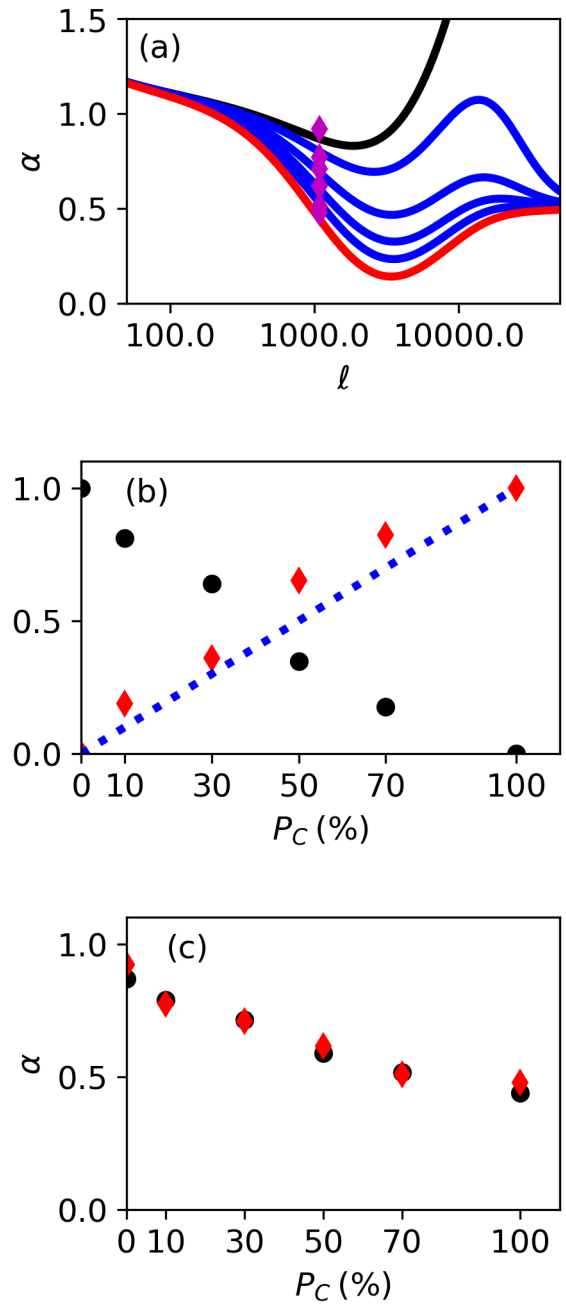


FIG. 8. (a) Calculated power-law local exponents as a function of step-length for different collision probabilities P_C (0%,10%, 30%, 70%, 100%, from top to bottom). Symbols are α values obtained from Monte Carlo simulations. (b) Percentage of photons that have escaped after step in case II (N_{II} , black circles) and case (III) (N_{III} , red diamonds) as a function of probability of collisions, P_C . (c) Comparison of α values obtained from simulated transmissions compared to estimated values of α_w , weighted with N_{II} and N_{III} .

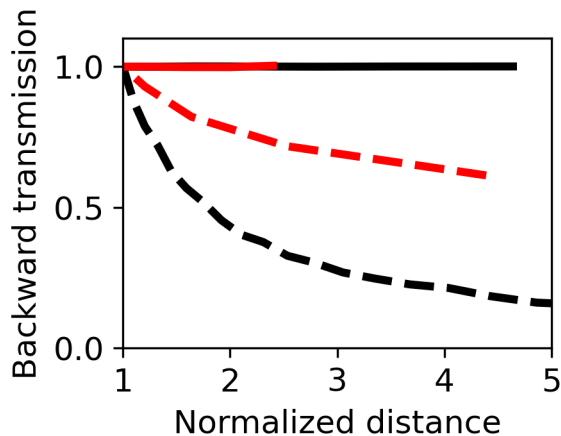


FIG. 9. Simulated backward transmission after the first scattering event. Black lines are for Double Pareto step-length distributions and red lines are for photon diffusion in atomic vapor. Solid lines are for diffuse transmission as a function of ℓ_0 and dashed lines are for diffuse transmission as a function of z_0 . Distance are normalized by the smaller value of ℓ_0 and z_0 and transmission is normalized by the value at minimum ℓ_0 or z_0 .

V. DISCUSSION

A. On the simulations

Two different results were found depending on the simulations: i) for transmission as a function of z_0 in the limit $\ell_0 \ll z_0$, the extracted α values do not depend on the size of the system L ; ii) for transmission as a function of ℓ_0 in the limit $z_0 \ll \ell_0$, the extracted α values depend on the size of the system and follow $\alpha = \alpha(\ell = L)$. The two cases have distinct behavior relative to the backward escape for the first step as we show in Fig. 9 for both Double Pareto and photon diffusion simulations. In case (i), the backward escape for the first step is very sensitive to the variable used z_0 and the forward transmission is ruled by this backward escape. As $z_0 \ll L$, it is natural to think that the forward transmission does not depend on L . In contrast, in case (ii), as the minimum step length is much higher than the starting point z_0 , the dependence of the backward escape after first step with the variable ℓ_0 is very smooth and α depends on the system size L .

B. Comparison between simulation and experiment

In the experiment, we have varied the starting point of the random walk z_0 , through the penetration depth of the laser, as a function of incident detuning. As detuning $x \neq 0$, the experiment corresponds to case (i) of the discussion in the previous section for which simulations have not shown a dependence of α with the size of the system. However, experiment has shown dependence with both cell length ($L = 1$ cm and $L = 2$ cm) and effective sys-

tem size ($L = 2$ cm for different atomic densities, see also [14]). Further investigations are needed to better understand those results. In simulations, α depends on the system size L if backward escape after first scattering is, almost, independent of the variable. Eventually, a mechanism not yet understood in the experiment might turn backward escape independent of incident detuning. Ideally, experimental investigation would require, a larger variety of cell thicknesses for the same density (more experimental points in Fig. 1). However, we disposed of only two good cells to perform the experiment.

C. On the experimental value of P_C

One curious result of the experiment is that the obtained values of α correspond to case III even though $P_C \ll 1$ (for instance, $P_C = 6\%$ for Fig. 1(a)). The value of P_C was estimated by calculating the collisional width as proportional to the density $\Gamma_C = kN$ with $k = 9 \times 10^{-8}$ Hz \cdot cm³ [31–33]. The density was estimated from fitting a theoretical curve to ballistic transmission (detected with photodetector PD1, see Fig. 1). However, impurities might be present in a vapor cell increasing the value of P_C . We have performed saturated absorption experiments to check that our cells have not a large amount of impurities and measured a homogeneous width of $\Gamma = 6.8 \pm 0.3$ MHz ($\Gamma = 1.3\Gamma_n$) at room temperature. Taking into account the extra width of $0.3\Gamma_n$ for the calculations of Γ_C the values of P_C would be of 27% for the density used in Fig. 1(a) and of 52% for the density used in Fig. 1(d). Those new values of P_C are not high enough to justify that the measured Lévy index is close to the case III curve, and it is still quite surprising from the atomic physics point of view to observe such a large effect of collisions (α values consistent with case III) even for $\Gamma_C < \Gamma_n$.

VI. CONCLUSIONS

We have investigated experimentally the light diffusion by a resonant atomic vapor which can be treated as a Lévy flight random walk [8, 10, 11, 16]. Emphasis is given to the fact that the walker alternates between two distinct step-length distributions, namely $P_{II}(\ell)$ and $P_{III}(\ell)$, which corresponds to case II and III of frequency redistribution, in the light scattering by vapor described by Hummer [18]. Each of the step-length distribution can be described locally as a power law with step-length-dependent Lévy index $\alpha(\ell)$. We have obtained the Lévy index α for different system sizes L and atomic densities from transmission measurement. The measured values correspond to those expected for a step with the length of the system size: $\alpha = \alpha(\ell = L)$.

We have simulated random walk with step-length distribution with local exponent that depends on the length of the step: (i) using a Double Pareto distribution and

(ii) simulating the photon diffusion in resonant vapor. Our emphasis in the simulations is to observe if the Lévy index extracted from diffuse transmission depends on the size of the system as in the experiment. Three parameters were relevant in the discussions: a typical step length ℓ_0 , the starting point of the random walk z_0 and the size of the system L . Analyzing the diffuse transmission as a function of z_0 for the limit $\ell_0 \ll z_0 \ll L$ [3, 4] (continuous limit) no dependence of Lévy index with system size was found. Analysing the diffuse transmission as a function of ℓ_0 for the limit $z_0 \ll \ell_0 \ll L$ [4], we extracted from simulation a system-size-dependent Lévy index, as in the experiment, that is, $\alpha = \alpha(\ell = L)$. The simulation results were similar for both step-length distributions proposed: Double Pareto and photon diffusion in atomic vapor.

The random walk for light in atomic vapors can be described as alternating between two distinct step-length distributions $P_{II}(\ell)$ and $P_{III}(\ell)$ with the first occurring with probability $(1 - P_C)$ and the last with probability P_C (P_C being the probability of atomic collisions during a light scattering event). The simulation of photon diffusion on atomic vapor has shown that Lévy index extracted from the scaling of the diffusive transmission depends on P_C . The extracted α value depends on the relative number of walkers that have escape the system after a step in $P_{II}(\ell)$ or $P_{III}(\ell)$.

In the experiment, the measured values of α are consistent with those expected for case *III* even for $P_C \ll 1$. For the atomic physics community it is intriguing to observe a signal related to atomic collisions (case *III*) even for $\Gamma_c \ll \Gamma_n$. Also, the experiment was analyzed by collecting diffuse transmission as a function of z_0 and a system-size-dependent Lévy index was measured. Further investigations are needed to understand the differences between experiment and simulations results, with probably a factor influencing the experiment not taken into consideration. In particular, the emergence of Case *III* characteristics in a regime of negligible collision probability ($P_C \ll 1$) challenges the standard interpretation of frequency redistribution and suggests an underlying mechanism that has yet to be fully understood.

This article presents a real physical system described by Lévy flight random walk that is more complicated than those usually modeled in the literature: local power exponent dependence on the step length and alternation between two Lévy-like step-length distributions. We are not aware of investigations of Lévy flights for systems with similar characteristics in the literature. We hope that both the experimental and simulation results presented here will encourage further investigation on similar non-usual Lévy flights random walk systems that might be important in non-ideal real systems.

ACKNOWLEDGMENTS

T.P.d.S. and J.P.L. acknowledge financial support from Conselho Nacional de Desenvolvimento Científico e Tecnológico, Brazil (CNPq, Public Call CNPq/MCTI/FNDCT N° 18/2021), Financiadora de Estudos e Projetos, Brazil (FINEP, N° 01.13.0235.07). I.C.N. acknowledge financial support from Coordenação de Aperfeiçoamento de Pessoal de Nível Superior, Brazil (CAPES).

DATA AVAILABILITY

The data that support the findings of this article are not publicly available. The data are available from the authors upon reasonable request.

APPENDIX: DETAILS OF THE EXPERIMENT

In the experiment, we used two distinct cells: one with thickness of $L = 1$ cm and the other with $L = 2$ cm. Both are glass cells with cylindrical shapes. The $L = 1$ cm cell has a diameter of 4.5 cm while the $L = 2$ cm cell has a diameter of 2 cm.

Each cell is heated by two independent ovens, one that determines the temperature of the vapor and the other that determines the temperature of a side-arm reservoir containing liquid cesium. The side-arm temperature determines the vapor pressure, while the vapor temperature determines the Doppler width and the Voigt parameter.

From experimental conditions of Fig. 1(a) to Fig. 1(d), side-arm temperature was risen to increase atomic density with a slight increase of vapor temperature with the Doppler width ranging from $\Gamma_D = 250$ MHz for density of $N = 3.5 \times 10^{12}$ atoms/cm³ (Fig. 1(a)) to $\Gamma_D = 268$ MHz for density of $N = 44 \times 10^{12}$ atoms/cm³ (Fig. 1(d)) corresponding to Voigt parameters values of $a = 10^{-2}$ and $a = 2 \cdot 10^{-2}$, respectively.

The laser used in the experiment is a semiconductor laser with external grating and is scanned around the $6S_{1/2}(F = 4) \rightarrow 6P_{3/2}(F' = 3, 4, 5)$ transitions. The beam has a diameter of 1.3 mm and its power is within the range of 1 to 9 μ W corresponding to intensities of 0.1 to 0.9 times the saturation intensity. For the intensity range used, the laser-vapor interaction is linear and no change in the Lévy index α with intensity was observed. The analyzes of diffuse transmission as a function of incident detuning are made in the range $-1.6 \leq x \leq -0.4$. The analyses are performed at the red side of the $6S_{1/2}(F = 4) \rightarrow 6P_{3/2}(F' = 5)$ transition to avoid the contribution of photons detected after a single scattering event (see [14] for more details). The limit $x \leq -0.4$ is to ensure a monotonic growth of T_D as a function of z_0 by avoiding the maximum of absorption coefficient around $x = -0.3$. The limit $-1.6 \leq x$ ensures

a effective frequency redistribution around the line center

[14, 24, 25].

-
- [1] P. Barthelemy, J. Bertolotti, and D. S. Wiersma. A lévy flight for light. *Nature*, 453:495–498, 2008.
- [2] Q. Baudouin, R. Pierrat, A.Eloy, E. J. Nunes-Pereira, P.-A.Cuniasse, N. Mercadier, and R. Kaiser. Signatures of lévy flights with annealed disorder. *Phys. Rev. E*, 90:052114, 2014.
- [3] S.V. Buldyrev, M. Gitterman, S. Havlin, A.Ya. Kazakov, M.G.E. da Luz, E.P. Raposo, H.E. Stanley, and G.M. Viswanathan. Properties of lévy flights on an interval with absorbing boundaries. *Physica A: Statistical Mechanics and its Applications*, 302(1):148–161, 2001. Proc. Int. Workshop on Frontiers in the Physics of Complex Systems.
- [4] J. Klinger, R. Voituriez, and O. Bénichou. Splitting probabilities of symmetric jump processes. *Phys. Rev. Lett.*, 129:140603, Sep 2022.
- [5] G. M. Viswanathan, V. Afanasyev, S. V. Buldyrev, E. J. Murphy, P.A. Princet, and H. E. Stanley. Lévy flight search patterns of wandering albatrosses. *Nature*, 381:413–415, 1996.
- [6] Jincui Li, Linxi Weng, Jie Xie, Jay Amrit, and Aymeric Ramiere. Lévy walk of quasiballistic phonons in nanowires. *Phys. Rev. E*, 105:064123, Jun 2022.
- [7] Tyler B Smith and Daniel B Weissman. Isolation by distance in populations with power-law dispersal. *G3 Genes—Genomes—Genetics*, 13(4):jkad023, 01 2023.
- [8] E. Pereira, J. M. G. Martinho, and M. N. Berberan-Santos. Photon trajectories in incoherent atomic radiation trapping as lévy flights. *Phys. Rev. Lett.*, 93:120201, 2004.
- [9] V. Zaburdaev, S. Denisov, and J. Klafter. Lévy walks. *Rev. Mod. Phys.*, 87:483–530, Jun 2015.
- [10] N. Mercadier, W. Guerin, M. Chevrollier, and R. Kaiser. Lévy flights of photons in hot atomic vapours. *Nat. Phys.*, 5:602–605, 2009.
- [11] N. Mercadier, M. Chevrollier, W. Guerin, and R. Kaiser. Microscopic characterization of lévy flights of light in atomic vapors. *Phys. Rev. A*, 87:063837, 2013.
- [12] Michelle O. Araújo, Thierry Passerat de Silans, and Robin Kaiser. Lévy flights of photons with infinite mean free path. *Phys. Rev. E*, 103:L010101, Jan 2021.
- [13] A. S. M. Macedo, J. P. Lopez, and T. Passerat de Silans. Sample size effects for lévy flight of photons in atomic vapors. *Phys. Rev. E*, 104:054143, Nov 2021.
- [14] J. P. Lopez, A. S. M. Macedo, M. O. Araújo, and T. Passerat de Silans. Dependence of lévy-flight transmission on the starting point for photons propagating in atomic vapors. *Phys. Rev. A*, 107:013501, Jan 2023.
- [15] A. R. Alves-Pereira, E. J. Nunes-Pereira, J. M. G. Martinho, and M. N. Berberan-Santos. Photonic superdiffusive motion in resonance line radiation trapping partial frequency redistribution effects. *J. Chem. Phys.*, 126:154505, 2007.
- [16] Martine Chevrollier. Radiation trapping and lévy flights in atomic vapours: an introductory review. *Contemporary Physics*, 53(3):227–239, 2012.
- [17] I.C. Nunes, M.O. Araújo, J.P. Lopez, and T. Passerat de Silans. Frequency redistribution and step-size distribution of light scattered by atomic vapor: Applications to lévy flight random walk. *Journal of Quantitative Spectroscopy and Radiative Transfer*, 343:109481, 2025.
- [18] David G. Hummer. Non-Coherent Scattering: I. The Redistribution Function with Doppler Broadening. *Monthly Notices of the Royal Astronomical Society*, 125(1):21–37, 07 1962.
- [19] H. Domke and I. Hubeny. Scattering of Polarized Light in Spectral Lines with Partial Frequency Redistribution: General Redistribution Matrix. *Astrophys. J.*, 334:527, November 1988.
- [20] W.R. Hindmarsh and Judith M. Farr. Collision broadening of spectral lines by neutral atoms. *Progress in Quantum Electronics*, 2:141–214, 1973.
- [21] Nicole Allard and John Kielkopf. The effect of neutral nonresonant collisions on atomic spectral lines. *Rev. Mod. Phys.*, 54:1103–1182, Oct 1982.
- [22] The comment on the convergence to Doppler profile or Voigt profile for cases II and III, respectively, is a simplification of the scattering dynamics to keep the main features of each case. A more detailed discussion involving the effect of the size of the system and the atomic electronic structure can be found in [17].
- [23] A. Omont, E. W. Smith, and J. Cooper. Redistribution of Resonance Radiation. I. The Effect of Collisions. *Astrophys. J.*, 175:185, July 1972.
- [24] H. A. Post. Radiative transport at the 184.9-nm hg resonance line. i. experiment and theory. *Phys. Rev. A*, 33:2003–2016, Mar 1986.
- [25] F Vermeersch, V Fiermans, J Ongena, H A Post, and W Wieme. Monte carlo investigation of imprisonment of resonance radiation with partial frequency redistribution. *Journal of Physics B: Atomic, Molecular and Optical Physics*, 21(10):1933–1937, may 1988.
- [26] Theoretical curves depend on the absorption Voigt profile parameter $a = (\Gamma_C + \Gamma_n)/\Gamma - D$ and thus depend on the atomic density, such that different theoretical curves should be drawn for each density.
- [27] Note that for each value of ℓ_0 there is a different step-length distribution defined in Eq. 8. For this reason, we change ℓ_0 over a small range to keep the step-length distribution approximately the same.
- [28] H. M. Anderson, S. D. Bergeson, D. A. Doughty, and J. E. Lawler. Xenon 147-nm resonance f value and trapped decay rates. *Phys. Rev. A*, 51:211–217, Jan 1995.
- [29] João Carlos de Aquino Carvalho and Thierry Passerat de Silans. Backward fluorescence of optically thick cs vapor: Experiment and monte-carlo simulations. *Journal of Quantitative Spectroscopy and Radiative Transfer*, 260:107469, 2021.
- [30] S. V. Buldyrev, S. Havlin, A. Ya. Kazakov, M. G. E. da Luz, E. P. Raposo, H. E. Stanley, and G. M. Viswanathan. Average time spent by lévy flights and walks on an interval with absorbing boundaries. *Phys. Rev. E*, 64:041108, Sep 2001.
- [31] Z.J. Jabbour, J. Sagle, R.K. Namiotka, and J. Huenekens. Measurement of the self-broadening rate coefficients of the cesium resonance lines. *Journal*

- of Quantitative Spectroscopy and Radiative Transfer, 54(5):767–778, 1995.
- [32] Tengfei Meng, Zhonghua Ji, Yanting Zhao, Liantuan Xiao, and Suotang Jia. Hyperfine dipole-dipole broadening of selective reflection spectroscopy at the gas-solid interface. Europhysics Letters, 115(6):63001, nov 2016.
- [33] Thierry Passerat de Silans. Determination of atomic density and collisional broadening of an alkali vapor by resonant interferometry. Journal of Physics B: Atomic, Molecular and Optical Physics, 51(19):195401, sep 2018.